Spatial distribution of cell–cell and cell–ECM adhesions regulates force balance while maintaining E-cadherin molecular tension in cell pairs

Joo Yong Sim[a,*,†], Jens Moeller[a,*], Kevin C. Hart[b], Diego Ramallo[c], Viola Vogel[d], Alex R. Dunn[c], W. James Nelson[b,e], and Beth L. Pruitt[a,e]

[a]Department of Mechanical Engineering, [b]Department of Biology, [c]Department of Chemical Engineering, and [e]Department of Molecular and Cellular Physiology, Stanford University, Stanford, CA 94305; [d]Department of Health Sciences and Technology, ETH Zurich, CH-8093 Zurich, Switzerland

ABSTRACT **Mechanical linkage between cell–cell and cell–extracellular matrix (ECM) adhesions regulates cell shape changes during embryonic development and tissue homoeostasis. We examined how the force balance between cell–cell and cell–ECM adhesions changes with cell spread area and aspect ratio in pairs of MDCK cells. We used ECM micropatterning to drive different cytoskeleton strain energy states and cell-generated traction forces and used a Förster resonance energy transfer tension biosensor to ask whether changes in forces across cell–cell junctions correlated with E-cadherin molecular tension. We found that continuous peripheral ECM adhesions resulted in increased cell–cell and cell–ECM forces with increasing spread area. In contrast, confining ECM adhesions to the distal ends of cell–cell pairs resulted in shorter junction lengths and constant cell–cell forces. Of interest, each cell within a cell pair generated higher strain energies than isolated single cells of the same spread area. Surprisingly, E-cadherin molecular tension remained constant regardless of changes in cell–cell forces and was evenly distributed along cell–cell junctions independent of cell spread area and total traction forces. Taken together, our results showed that cell pairs maintained constant E-cadherin molecular tension and regulated total forces relative to cell spread area and shape but independently of total focal adhesion area.**

Monitoring Editor
Margaret Gardel
University of Chicago

Received: Dec 15, 2014
Revised: May 5, 2015
Accepted: May 5, 2015

INTRODUCTION

Studies in single cells have revealed that key proteins of integrin-based adhesions act as mechanotransducers between the extracellular matrix (ECM) and the actomyosin cytoskeleton (Schoen *et al.*, 2013). Conversely, how multicellular tissues respond to mechanical forces transmitted through cadherin-based cell–cell junctions is poorly understood and represents a critical knowledge gap. This balance of mechanical interactions at cell–cell junctions and cell–ECM adhesions governs basic processes in development and disease. For example, changes in mechanical forces at cell–cell and cell–ECM adhesions coordinate the collective migration of epithelial sheets during development (Cai *et al.*, 2014), folding of epithelial sheets into tubes, and maintenance of tissue and organ homeostasis (Halbleib and Nelson, 2006; Friedl and Gilmour, 2009).

Cellular forces are regulated by actomyosin-generated tension, which depends on cell size and shape (Vogel and Sheetz, 2006). Tan *et al.* (2003) showed that single cells generate higher traction forces on larger patterns on micropost arrays Although substrate rigidity affects cell spreading and force generation (Ghibaudo *et al.*, 2008), Tee *et al.* (2011) showed that the shape and size of human mesenchymal stem cells can also control stem cell differentiation. Rape *et al.* (2011) found that traction stresses on the ECM are increased in larger

This article was published online ahead of print in MBoC in Press (http://www.molbiolcell.org/cgi/doi/10.1091/mbc.E14-12-1618) on May 13, 2015.

*These authors contributed equally and should be regarded as joint first authors.

†Present address: Bio-Medical IT Convergence Research Department, Electronics and Telecommunications Research Institute, Daejeon, 305-700, Republic of Korea.

Address correspondence to: Beth L. Pruitt (pruitt@stanford.edu).

Abbreviations used: EcadTSMod, E-cadherin tension sensor module; ECM, extracellular matrix; FBS, fetal bovine serum; FLIM, fluorescence lifetime imaging microscopy; FRET, Förster resonance energy transfer; GFP, green fluorescent protein; MDCK, Madin–Darby canine kidney; PAA, polyacrylamide; PDMS, polydimethylsiloxane.

and more elongated cells. Recently, Oakes *et al.* (2014) proposed a mechanical model of adherent cells as contractile gels from experimental observations that cell spread area regulated cell-generated strain energy; further, this strain energy was independent of substrate stiffness, the number of focal adhesions, or cell aspect ratio.

In contrast to these studies of single cells, few studies have examined the force balance between cell–cell and cell–ECM adhesions in pairs of cells. Maruthamuthu *et al.* (2011) reported that cell–ECM forces correlated positively with cell–cell adhesion forces using unpatterned epithelial cell pairs on flat, deformable polyacrylamide (PAA) gel substrates with embedded fiducial markers for traction force microscopy (TFM). Studies of endothelial cell pairs patterned in bowtie shapes on micropost arrays by Liu *et al.* (2010) found that cell–cell forces correlated with cell–cell contact length but not with cell–ECM forces. Finally, Tseng *et al.* (2012) patterned epithelial cell pairs on TFM gels using I-shapes and squares and found that cell pairs positioned cell–cell junctions across the I-shapes in the ECM-deprived regions to achieve stable, low-energy configurations that minimized cell–cell and cell–ECM forces. However, different cell types, TFM substrates, and spatial constrains of cell spread area and cell–ECM adhesions were used in these studies, and thus it is difficult to compare the interdependence of cell–cell and cell–ECM forces in cell pairs.

Cell–cell junctions in most epithelial cells are formed by cadherins (Takeichi, 2014). Cadherins facilitate homotypic cell–cell adhesion through *trans* interactions of the extracellular domain (Chu *et al.*, 2004) and regulate mechanical interactions between cells through intracellular interaction with the actin cytoskeleton via α-catenin and associated actin-binding proteins (Takeichi, 2014). A variety of experimental approaches have suggested mechanoregulation of E-cadherin at epithelial cell–cell junctions. A Förster resonance energy transfer (FRET)–based tension biosensor has been used to show that E-cadherin is under actomyosin-generated tension at cell–cell junctions (Borghi *et al.*, 2012; Engl *et al.*, 2014; reviewed in Barry *et al.*, 2014), and this tension transiently increased with applied external force (le Duc *et al.*, 2010; Borghi *et al.*, 2012). Disrupting calcium-dependent E-cadherin binding with low-calcium media reduced cell–cell forces (Maruthamuthu *et al.*, 2011). Twisting force cytometry of E-cadherin–coated beads bound to E-cadherin on the surface of epithelial cells resulted in cell stiffening correlated with the recruitment of vinculin to the plasma membrane at the site of bead attachment (le Duc *et al.*, 2010; Twiss *et al.*, 2012) and also depended on actomyosin activity and accessibility of a cryptic binding site in α-catenin (Yonemura *et al.*, 2010). Although the cadherin complex is linked to actin via α-catenin, the affinity of the cadherin ternary complex with actin is weak, based on in vitro cosedimentation assays (Drees *et al.*, 2005; Yamada and Nelson, 2007). Of importance, linkage of the cadherin–catenin complex to the actin cytoskeleton requires actomyosin-dependent forces (reviewed in Barry *et al.*, 2014), and piconewton forces stabilize α-catenin–actin filament bonds via a catch-bond mechanism (Buckley *et al.*, 2014).

In single cells, substrate deformations can be readily linked to forces transmitted through cell–ECM adhesions using traction force microscopy methods (Schoen *et al.*, 2013). In cell pairs, different concepts have been suggested to deconvolve the force balance between cell–ECM and cell–cell junctions. Liu *et al.* (2010) first inferred forces across cell–cell junctions using polydimethylsiloxane (PDMS) micropost arrays. In the absence of inertia, all cellular mechanical forces were in static balance at all times. Thus, within cell pairs, the net traction force exerted on the substrate, as measured by micropost deflection, defined an "intercellular tugging force." Tseng *et al.* (2012) later defined "intercellular" and "intracellular" forces as estimates of cell–cell and cell–ECM forces using TFM on PAA gels. Based on the orientation of the traction force components, forces perpendicular to the cell–cell junction were defined as intercellular forces, whereas forces parallel to the junction served as proxy for cell–ECM forces. Similarly, Maruthamuthu *et al.* (2011) calculated endogenous "cell–cell forces" at cell–cell junctions as the vector sum of all traction forces under each cell using TFM. "Cell–ECM forces" in those unrestricted cell pairs were calculated as the sum of traction force magnitudes perpendicular to the cell–cell force vectors. To analyze mechanical stresses between a cell and its neighbors in multicellular epithelial cell sheet monolayers, monolayer stress microscopy was developed (Tambe *et al.*, 2011). To calculate intercellular stress between cells, a cell sheet was assumed to have certain elastic material properties, heights, and mechanical boundary conditions that were valid for commonly used in vitro monolayer systems and were in agreement with a theoretical model based on molecular dynamics simulations (Tambe *et al.*, 2013; Zimmermann *et al.*, 2014).

In this work, we asked whether cell spread area and shape regulate the force balance in cell pairs and whether changes in the force directed across cell–cell junctions modulated E-cadherin load bearing. We observed pairs of Madin–Darby canine kidney (MDCK) cells adhered to micropatterned ECM proteins in rectangles and I-shapes of increasing size and aspect ratio. We asked whether 1) total traction forces and strain energies increase as a function of increased spread area in cell pairs, 2) the spatial distribution of cell–ECM and cell–cell adhesion modulates the force balance, and 3) molecular tension on E-cadherin increases as force directed across cell–cell junctions increases. We calculated the total force exerted by the cell pair as sum of all traction force magnitudes under both cells. Total strain energies are derived from the total forces as described by Oakes *et al.* (2014). We define cell–cell *forces* as the vector sum of all traction forces under each cell in a cell pair and cell–ECM *forces* as the sum of traction force magnitudes perpendicular to cell–cell force vector as described by Maruthamuthu *et al.* (2011).

We observed that total forces and strain energies strongly correlated with the spread area of cell pairs. The strength of this trend depended on the spatial pattern of ECM but was independent of the focal adhesion area. We also found that molecular-scale tension on E-cadherin remained constant independent of cell spread area, total traction forces, or the force balance at cell–ECM and cell–cell adhesions. Our results indicate that the spatial pattern of cell–ECM adhesions controls the force balance in multicellular interactions. Related to these shape changes, cell pairs regulate junction length and E-cadherin density along the junction as the force balance perpendicular and parallel to the junction is varied.

RESULTS

Constraining the shape of cell pairs and deriving cell-generated traction forces

We constrained the spatial distribution of cell–ECM adhesions and resulting cell–cell junction lengths in pairs of MDCK epithelial cells by patterning ECM on PAA hydrogels with micrometer resolution (Supplemental Figure S1A; see *Materials and Methods*). Pairs of MDCK cells attached and formed focal adhesions at the pattern edges. We observed focal adhesions via the distribution of green fluorescent protein (GFP)–paxillin, which localized to cell–ECM adhesions (Supplemental Figure S1B). Cell–cell junctions, observed by the distribution of E-cadherin–DsRed, formed across the space between the adhesive regions of the pattern (Supplemental Figure S1B). To quantify cell-generated traction forces, we used cell-generated substrate deformations by tracking fluorescent beads mixed into the PAA gels (see *Materials and Methods*; Butler *et al.*, 2002; Maruthamuthu *et al.*, 2011; Tseng *et al.*, 2012). Substrate patterning

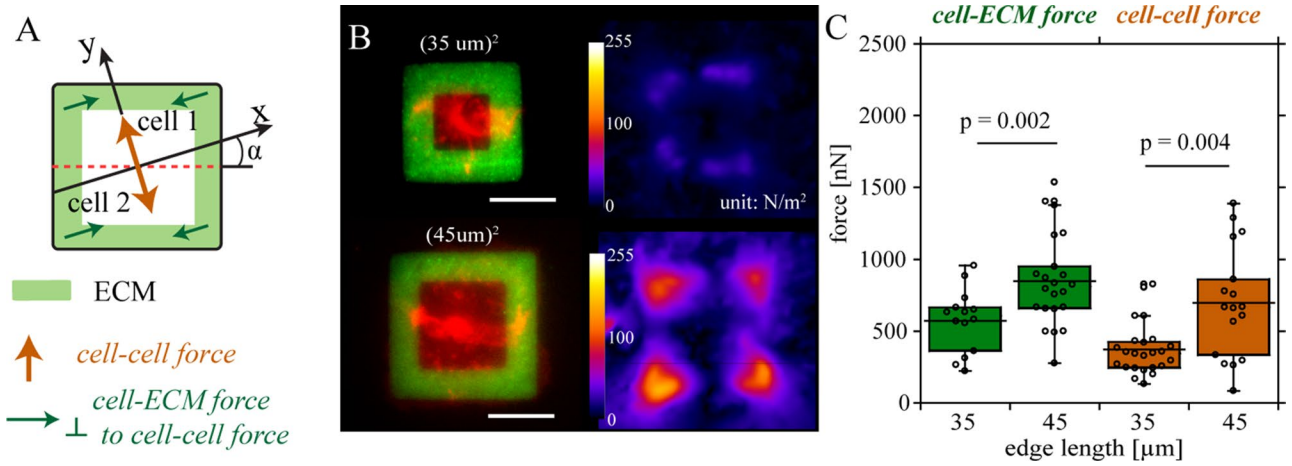

FIGURE 1: Cell–cell and cell–ECM forces in cell pairs increased with increased spread area on square patterns. (A) To compare across patterned cell pairs, we defined an *x*-*y* coordinate system relative to the cell–cell junction and only analyzed pairs having *x*-axes within $\alpha \pm 30°$. To estimate the cell–cell force balanced across cell pairs, we integrated the traction force vectors under each cell, $\sum \vec{F}_i$ (A). To estimate cell–ECM forces that are least dependent on cell–cell forces, we integrated the force magnitudes perpendicular to the cell–cell force vector, $\sum |F_{\perp,i}|$. (B) Pairs of E-cadherin–DsRed MDCK cells spread fully on squares containing collagen I and gelatin–Alexa Fluor 488 (green). Cell pairs on larger squares generated larger total forces. (C) Cell-cell and cell–ECM forces for MDCK cell pairs on 35- and 45-μm patterns. Scale bar, 20 μm.

enabled comparison across multiple cell pairs with similar shape, spread area, and junction orientations. We defined a local coordinate system for each cell pair relative to the orientation of the cell–cell junction (Figure 1A). To compare similar geometries, we limited our analysis to cell pairs with *x*-axes consistently oriented ±30° from the frame coordinates. We summed the magnitude of traction forces across cell pairs, $\sum |\vec{F}_i|$, to derive the total in-plane traction force generated by both cells. For each cell in a pair, we calculated the forces balanced across cell pairs, that is, the cell–cell force, as the vector sum of all traction forces for each cell, $\sum \vec{F}_i$ (Figure 1A). This cell–cell force on average was oriented perpendicular to the cell–cell junction (Supplemental Figure S2). We integrated the force magnitudes perpendicular to the cell–cell force vector, $\sum |F_{\perp,i}|$, to estimate cell–ECM force exerted at the focal adhesions. For all forces, the mean and SEM are provided.

Cell–cell and cell–ECM forces increase with isometric dilation of spread area on square frames

We tested whether pairs of MDCK cells attached to square micropatterns exerted larger tractions, as in single cells, when the edge dimension of square patterns was increased from 35 μm (small) to 45 μm (large; Figure 1B). MDCK cell pairs did not reliably fill patterns >45 μm. As expected, traction stresses localized mainly at the corners of cell pairs, and cell pairs on large patterns exerted larger traction stresses (Figure 1B). The traction fields overlapped the distributions of integrin-based focal adhesions (Supplemental Figure S1B). When cell spread area increased 1.7-fold, cell pairs exerted higher cell–ECM and cell–cell forces (Figure 1C): cell–ECM forces increased 1.5-fold (573 ± 218 to 848 ± 319 nN), and cell–cell forces almost doubled (372 ± 180 to 696 ± 386 nN). This behavior is consistent with increased traction stresses observed in single fibroblasts on ECM patterns of different sizes (Oakes *et al.*, 2014). To test whether the cell–cell force correlated with the fluorescence intensity of E-cadherin–DsRed at the cell–cell junction, we calculated the Pearson's ρ for a scatter plot of cell–cell force and the average E-cadherin–DsRed fluorescence intensity (Supplemental Figure S3). Cell-cell force correlated weakly with E-cadherin levels for cell pairs on square micropatterns (ρ = –0.24 for 35 × 35 μm squares, 0.37 for 45 × 45 μm squares, and –0.14 for pooled data).

Cell–cell and cell–ECM forces increase on elongated rectangular frame patterns

We next tested whether elongating square patterns into rectangles with increased area (from 35 × 35, to 35 × 45, to 35 × 60 μm) increased cell–cell and cell–ECM forces (Figure 2A). When the aspect ratio was increased from 1:1 (35 × 35 μm) to 1:1.3 (35 × 45 μm), we observed no significant increase in either cell–cell or cell–ECM force (Figure 2B). However, both forces increased on rectangles with an aspect ratio of 1:1.7 (35 × 60 μm): cell–ECM forces increased almost 1.4-fold (625 ± 293 to 846 ± 167 nN), and cell–cell forces increased 2.5-fold (372 ± 180 to 935 ± 260 nN; Figure 2B). For comparison, the 35 × 60 μm rectangles had about the same area as the 45-μm squares, and cell–cell and cell–ECM forces on both patterns were almost identical. These data support the idea that traction forces scale with spread area not only in single cells (Oakes *et al.*, 2014) but also in cell pairs. As expected in these peripherally anchored cell pairs, junction length did not change significantly with increasing aspect ratio (Figure 2C).

We then asked whether these increases in cell–cell force resulted in increased recruitment of E-cadherin to the cell–cell junction. We measured the average and integrated E-cadherin–DsRed fluorescence intensity along the cell–cell junction of cell pairs on large rectangles and squares (average intensities normalize for junction length differences). The average and integrated E-cadherin–DsRed intensity did not vary between cell pairs on large and small squares (Supplemental Figure S4). Surprisingly, the average intensity *decreased* by >50% in cell pairs on 1:1.7 rectangles relative to small squares (Figure 2D). These data indicate that cell pairs do not recruit more E-cadherin in response to chronic elevation of cell–cell forces.

Cell–cell force increases but cell–ECM force is constant on isometrically larger I-shapes

On rectangles, the edges of cell–cell junctions were anchored by cell–ECM adhesions at the pattern periphery. To test whether

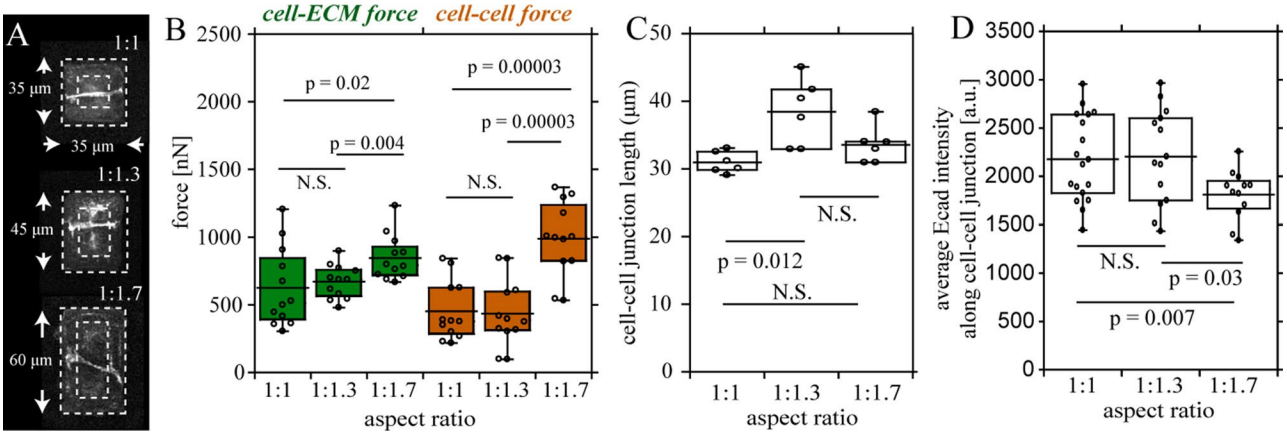

FIGURE 2: Cell-cell and cell–ECM forces increased in cell pairs on elongated rectangles. (A) E-cadherin–DsRed MDCK cell pairs on rectangles with varied aspect ratios (dotted outline). (B) Cell-cell and cell–ECM forces increased as the aspect ratio changed from 1:1: to 1:1.7. (C) Cell-cell junction length remained constant for cell pairs on elongated rectangles. (D) Average E-cadherin intensity in cell–cell junctions decreased as the aspect ratio of rectangular patterns increased.

removing ECM anchorage at the ends of the cell–cell junctions changed the balance of cell–cell and cell–ECM forces, we patterned cell pairs on I-shapes (Tseng *et al.*, 2012) of different sizes (Figure 3A). As expected, focal adhesions to the ECM localized predominantly at the bar ends of the I-shapes away from the cell–cell junction (Figure 3B). Both cell–cell and cell–ECM forces increased in 35 × 35 μm (small) I-shape patterns relative to the small squares (Figures 1 and 3): cell–ECM forces increased 1.2-fold (573 ± 218 nN [square] to 705 ± 336 nN [I-shape]), and cell–cell forces increased 1.6-fold (372 ± 180 nN [square] to 611 ± 314 nN [I-shape]), while the cell–cell junction length decreased from 31 to 22 μm. As with the square patterns, we also increased the edge length of the I-shapes 1.3-fold from 35 to 45 μm (Figure 3A): cell–ECM forces increased a significant 1.4-fold (705 ± 336 to 968 ± 464 nN); however cell–cell forces did not increase significantly (611 ± 314 to 742 ± 438 nN; Figure 3C). Cell–cell junction length also increased 1.3-fold on the isometrically larger I-shapes (Figure 3D). The average E-cadherin intensity along the cell–cell junction decreased by ~50% (Figure 3E), but the integrated E-cadherin intensity remained constant. These results indicate that E-cadherin recruitment and cell–cell junction length are independent of changes in endogenous forces.

Cell–cell and cell–ECM forces remain constant on elongated I-shapes

Both cell–cell and cell–ECM forces increased in cell pairs on 1:1.7–aspect ratio rectangles relative to small squares (Figure 2B). In contrast, cell–cell and cell–ECM forces remained constant on elongated I-shapes (Figure 4B). On elongated I-shapes, the cell–cell junction length decreased ~50% (Figure 4C), and although the average E-cadherin–DsRed intensity did not change significantly (Figure 4D), the integrated E-cadherin intensity decreased by ~50%. These results indicate that cell–ECM adhesions at the distal ends of cell–cell junctions, as in the rectangle patterns, are required to maintain cell–cell junction length and support proportional increases in cell–cell and cell–ECM forces. These results are in agreement with the elevated tension observed in nonadhesive bridge regions for single cells on ECM stripes (Rossier *et al.*, 2010).

Total forces and strain energies are regulated by the spread area of cell pairs and cell–ECM constraints

The increase in cell–cell forces on elongated rectangle patterns compared with elongated I-shapes supports the idea that spread area (with increases supported by cell–ECM adhesions at the distal ends

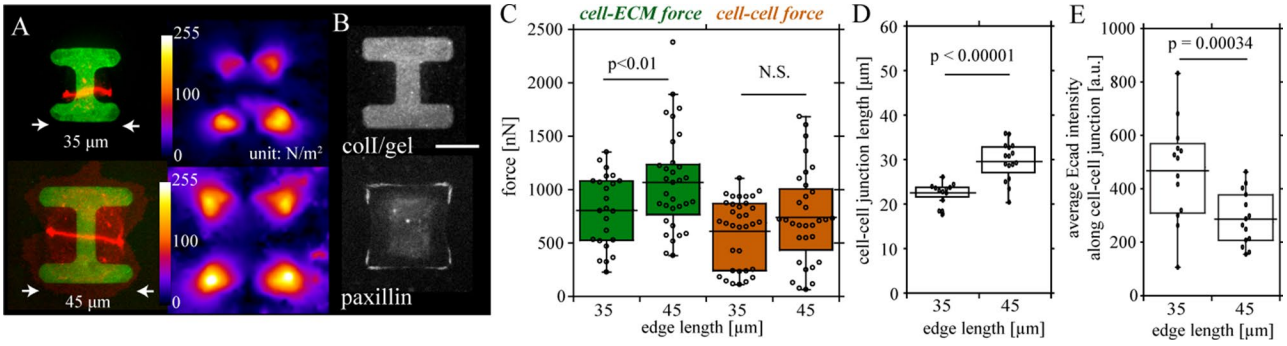

FIGURE 3: Cell–ECM force increases but cell–cell force remains constant on dilated I-shapes. (A) Pairs of E-cadherin-DsRed MDCK cells fully spread on I-shapes of different aspect ratios (green). Traction stress heat maps are estimated from bead displacements. (B) Focal adhesions localized to the corners of I-shapes under paxillin-GFP MDCK cells and were excluded under the cell–cell junction (scale bar, 20 μm). (C) Cell pairs on the larger I-shapes generate larger cell–ECM force but not cell–cell force. (D, E) Cell-cell junction length increased but average E-cadherin intensity along cell–cell junction decreased with increasing pattern sized.

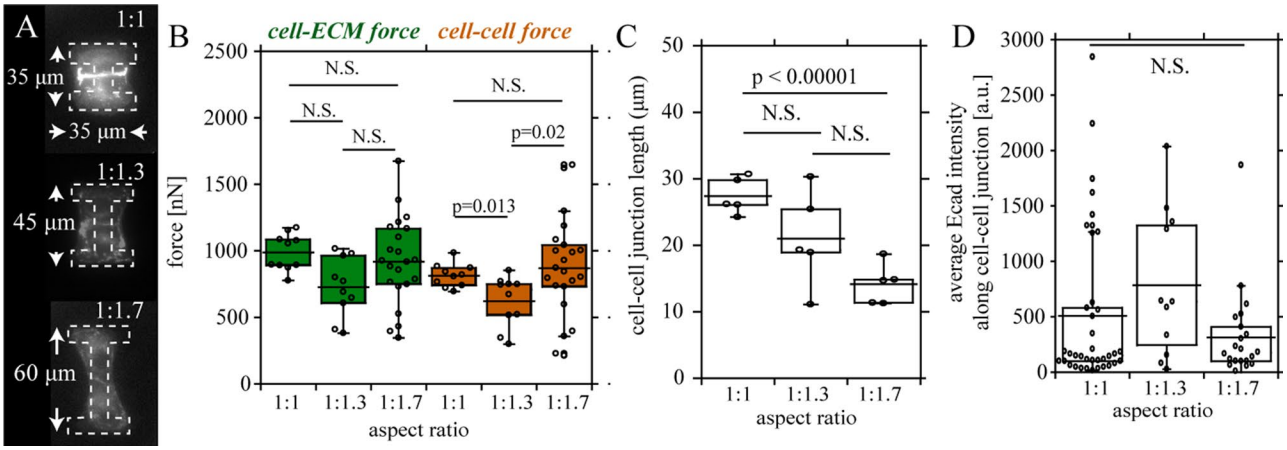

FIGURE 4: Cell-cell force remains constant with elongation of I-shapes. (A) E-cadherin–DsRed MDCK cell pairs patterned on I-shapes with increasing aspect ratio (dotted outline). (B) Cell–cell and cell–ECM forces did not vary significantly with variation of I-shape aspect ratio. (C) Cell–cell junction length decreased with elongation of I-shapes. (D) Average E-cadherin intensity remained constant on I-shapes with different aspect ratio.

of cell–cell junction) plays an important role in determining the force balance in cell pairs. We next tested whether increased cell–cell forces also correlated with increased strain energies and total forces with increasing spread area in cell pairs. The total force of both cells in a cell pair is the integral of force magnitudes, $\sum|\bar{F}_i|$, and strain energy is calculated as described by Oakes *et al.* (2014) (see *Materials and Methods*). Total force, strain energy, and spread area of cell pairs increased proportionally as the pattern size increased in squares and rectangles. As expected, total force, strain energy, and spread area of cell pairs remained constant on I-shapes of all aspect ratios (Figure 5). Of note, total forces on all sizes of I-shapes were as high as forces on the largest 1:1.7 rectangles, even though cell spread areas were significantly larger on rectangles (Figure 5, A and C). These data indicate that total forces and strain energies in cell pairs are determined not only by cell spread area but also by the spatial constraints placed on cell–ECM interactions, especially under the cell–cell junction. Although external ECM patterns drove increased cell spread area accompanied by proportional increases in total force and strain energy, the integrated focal adhesion area remained constant for patterns of cell pairs (Figure 5D), similar to observations on elongated single cells (Oakes *et al.*, 2014).

Cells in pairs exert larger forces than single cells of the same size

To examine the role of cell–cell junctions in regulating total forces and strain energy, we compared the total force in single cells and cell pairs confined to the same spread area on 35-μm-square patterns (1225 μm^2). Single MDCK cells could not fill larger patterns. We found 2.5-fold higher total forces and 5-fold higher strain energies for cell pairs than with single cells (Figure 5, E and F). Total force and strain energy for each cell in a pair of cells on 35 × 60 μm rectangles (1050 μm^2/cell) were also larger (2.2-and 5.7-fold, respectively) than in single cells of comparable spread area. These data indicate that the presence of a cell–cell contact coordinates increased cell generated traction forces and endogenous strain energies.

E-cadherin maintains molecular tension homeostasis under a wide range of endogenous cell–cell and cell–ECM forces

We observed that the spatial distribution of cell–ECM adhesions and cell spread area controlled cell–cell and cell–ECM forces in cell pairs. However, increasing cell–cell forces did not recruit increased amounts of E-cadherin to the cell–cell junction. Thus we asked whether increased cell–cell forces correlated with increased molecular tension in E-cadherin. We used a FRET-based tension biosensor engineered in the cytoplasmic domain of E-cadherin (EcadTSMod; Figure 6A), which we described and characterized previously (Grashoff *et al.*, 2010; Borghi *et al.*, 2012). FRET efficiency was calculated from fluorescence lifetime measurements of the FRET donor mTFP1 (see *Materials and Methods*). The baseline FRET efficiency for full-length EcadTSMod was ~18% in MDCK cells on adhesive, unpatterned gels (Figure 6A). We confirmed that EcadTSMod was sensitive to actomyosin-generated cellular tension: 1) EcadTSMod (Δcyto), lacking the β-catenin–binding domain and linkage to α-catenin and F-actin, caused a ~4% increase in FRET (Figure 6A), as in Borghi *et al.* (2012); and 2) addition of cytochalasin D (CD; 0.5 μM) to disrupt the actin cytoskeleton resulted in a ~4% increase in FRET. A 4% change represents a per-molecule force decrease of ~0.7 pN based on a previously reported calibration of TSMod (Grashoff *et al.*, 2010).

We expected an increase in EcadTSMod molecular tension in all cases because on elongated rectangles, the average fluorescence intensity of E-cadherin–DsRed at cell–cell junctions decreased, while spread area and cell–cell forces increased (Figure 2), and on I-shapes, the junction length decreased, while cell–cell force and E-cadherin intensity remained constant (Figure 4). Surprisingly, EcadTSMod FRET efficiency remained constant in cell pairs cultured on rectangles and I-shapes of all aspect ratios (Figure 6B). EcadTSMod FRET efficiency was independent of cell–cell force, cell–cell junction length, and E-cadherin levels at cell–cell junctions. A parsimonious explanation is that E-cadherin is maintained under a constant tension required for cytoskeletal engagement, and this molecular tension is independent of overall cell forces (Borghi *et al.*, 2012; Buckley *et al.*, 2014). Thus we asked whether desmosomes, another load-bearing cell–cell adhesion complex, were recruited with increasing cell–cell forces. We used indirect immunofluorescence of desmoplakin, a protein found in desmosomes, in cell pairs on elongated I-shapes having constant cell–cell forces but decreasing junction lengths (see *Materials and Methods*). The average and integrated fluorescence intensity of desmoplakin *decreased* in elongated cell pairs on I-shapes (Supplemental Figure S5). We then tested whether there was a correlation between E-cadherin fluorescence intensity and E-cadherinTSMod FRET efficiency. We generated a scatter plot of average E-cadherin intensity versus E-cadherinTSMod FRET efficiency of all shapes and aspect ratios (Supplemental Figure S6) but found a weak correlation ($\rho = -0.29$).

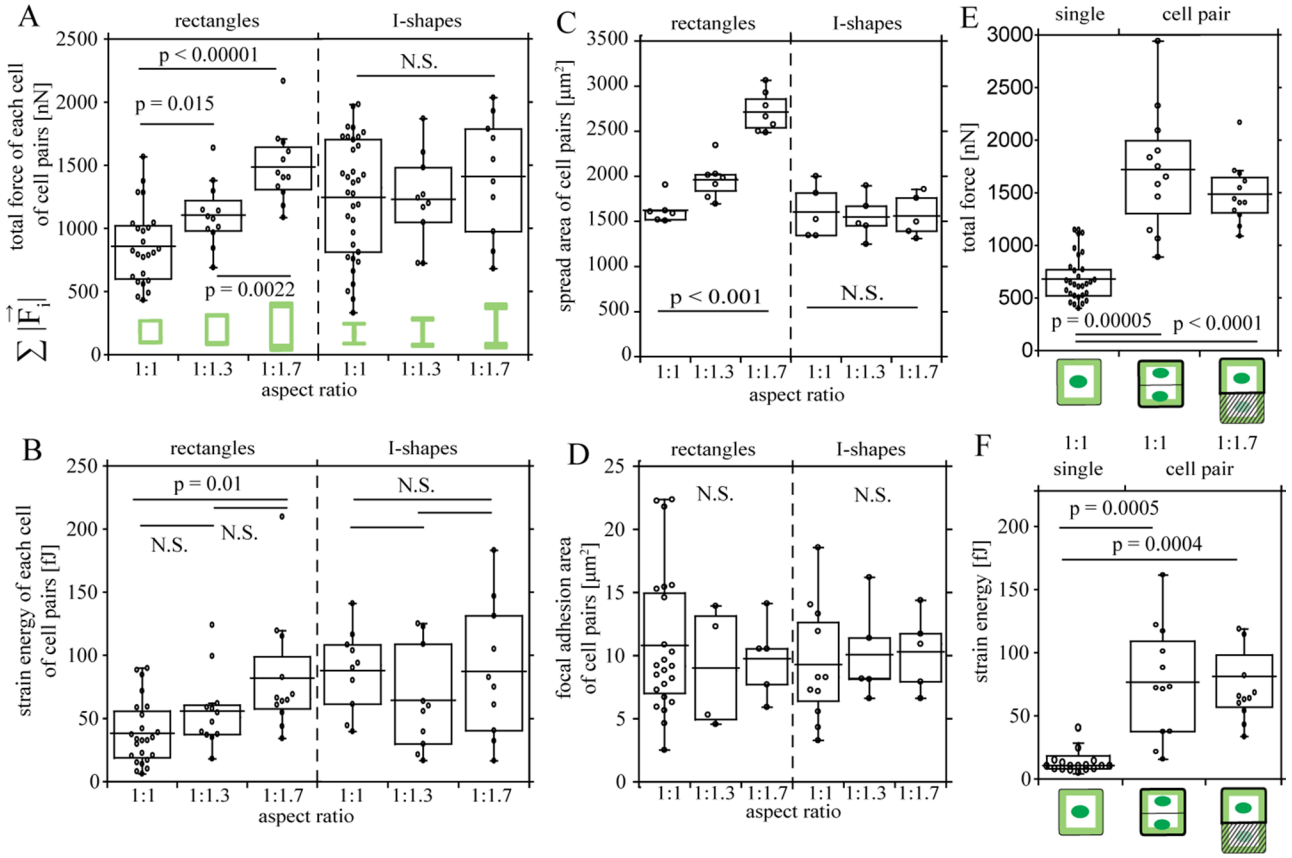

FIGURE 5: Total cell forces regulated by cell spread area and spatial pattern of cell–ECM adhesions. (A) Total force per cell increased with increasing aspect ratio from 1:1 to 1:1.7 on rectangles but remained constant for I-shapes. (B) Strain energy of each cell in MDCK cell pairs on rectangle and I-shape patterns with varied aspect ratio. (C) Spread area on rectangles increased proportionally to aspect ratio but remained constant on I-shapes. (D) The integrated area of focal adhesions (from fluorescently labeled paxillin) remained constant regardless of aspect ratio and the shape of the ECM pattern. (E, F) Total forces and strain energies for single cells and cell pairs on the 35-μm-square patterns and for each cell in a cell pair on 35 × 60 μm rectangles.

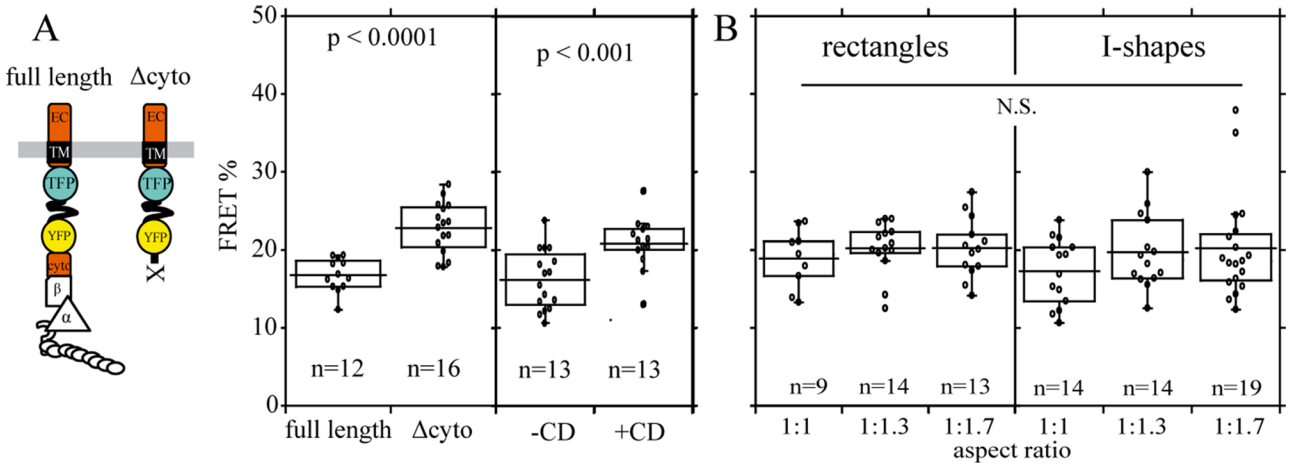

FIGURE 6: Direct measurements of E-cadherin cytoplasmic tension and actin organization on different patterns. (A) FRET sensor (TSMod) engineered into the cytoplasmic domain of E-cadherin. FRET efficiency increased from 18% for the full-length EcadTSMod to 23% for the control construct lacking the cytoplasmic domain. The FRET efficiency increased by the same amount when cells were treated with cytochalasin D, confirming that the EcadTSMod was sensitive to actomyosin-generated tension. (B) EcadTSMod FRET efficiency at cell–cell junctions in cell pairs cultured on rectangular and I-shapes with different aspect ratios. FRET signal was not significantly different between these samples.

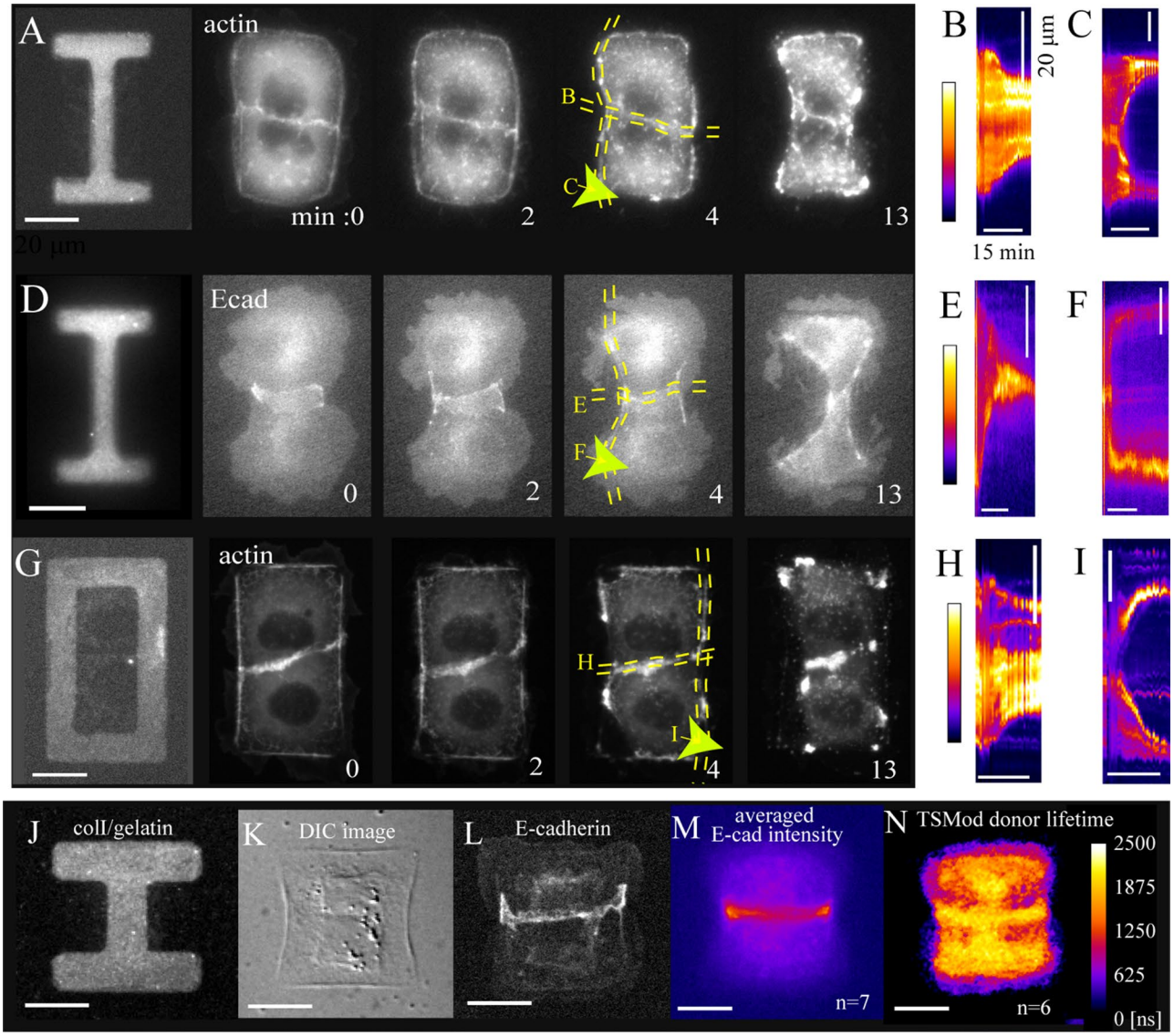

FIGURE 7: E-cadherin localized at the distal ends of cell–cell junctions with a uniform distribution of EcadTSMod tension. (A, D, G) Actin and E-cadherin dynamics in the presence of 0.5 μM CD on I-shape and rectangular patterns. (B, E, H) Kymographs of actin and E-cadherin show shrinkage of stress fibers and the junction upon CD treatment. (C, F, I) Kymographs of actin and E-cadherin asters show retraction after CD treatment. (J–L) ECM, differential interference contrast, and E-cadherin images of MDCK cell pair on I-shape (scale bar, 15 μm). (M) Average E-cadherin–DsRed intensities on I-shape ($n = 7$) were highest at the ends of the junction. (N) The average lifetime mTFP1 (donor) in EcadTSMod cells spreading on the I-shapes was evenly distributed along the cell–cell junction (n = 6).

The actin cytoskeleton is under elevated tension at the distal ends of cell–cell junctions

Higher intensities of E-cadherin–DsRed at the distal ends of cell–cell junctions indicated a nonuniform "stress" distribution at the junction. Thus we postulated that E-cadherin might distribute molecular tensions over more molecules in regions where cell–cell forces were higher. To identify sites of high actin contractility, we added low concentrations of CD (0.5 μM) to cap the barbed ends of actin filaments. This treatment results in displacement of actin bundles from putative anchorage points on the membrane (Yamada and Nelson, 2007). To exclude effects of cell–ECM adhesions on actin bundle dynamics at the distal edges of cell–cell junctions, we first analyzed actin-GFP in cell pairs on elongated (1:1.7) I-shapes (Figure 7, A–C). Two minutes after CD addition, cell–cell junctions began to shorten, actin bundles started to recoil from the distal edges of cell–cell contacts (Figure 7A), and a large fraction of E-cadherin simultaneously retracted from the junction (Figure 7D). Retraction velocities away from the junction were similar for actin-GFP and E-cadherin–DsRed (Figure 7, B and E). Thirteen minutes after CD treatment, cortical actin bundles had dissolved, and foci of actin were localized to the corners of the cell–ECM adhesions (Figure 7A). During this time, the cell–cell junctions shortened significantly, but the contact remained intact.

To test whether the recoil dynamics of actin bundles was controlled by myosin activity, we treated cells with ML-7, which inhibits myosin light chain kinase and thus myosin activation. Adding ML-7 for 20 min had little or no detectable effect on the distribution of actin bundles or E-cadherin (Supplemental Figure S7). When CD was added in the presence of ML-7, the retraction rates of actin bundles and E-cadherin were similar to those in cells treated with only CD (Supplemental Figure S7). These results indicate that cortical actin bundles are under constitutive (nonmyosin) tension

and recoil in the presence of CD. This built-in tension develops during maturation of cell–cell junctions and cell spreading.

Next we added CD to cells cultured on rectangle patterns to test whether cell–ECM adhesion underneath cell–cell junctions changed the contractility of cortical actin bundles. CD addition still caused actin bundle retraction to the distal end of cell–ECM adhesions (Figure 7, G and I), similar to that in CD-treated cells on the I-shape patterns. However, the constrained cell–cell junction did not shorten as much as that in cells on I-shapes (Figure 7H). These results further support the idea that cortical actin bundles are embedded proximal to the plasma membrane at the edges of cell–cell junctions and have a tight association with the E-cadherin complex. We conclude that cell–cell force is highly localized at the ends of cell–cell junctions and is distributed nonuniformly along the cell–cell junction.

E-cadherin localizes to the high stress regions at the ends of cell–cell junctions

We next asked whether E-cadherin plays a role in the spatial localization of tension at the distal ends of cell–cell junctions. We overlapped E-cadherin–DsRed fluorescence intensity micrographs of fluorescence lifetime imaging microscopy (FLIM)-FRET data from cell pairs patterned on 35-μm I-shapes (Figure 7). Cell pairs on I-shapes exhibited less variation in cell–cell junction angle and size than on rectangular patterns (Tseng *et al.*, 2012). Consistent with the CD experiments, we observed more E-cadherin localized at the distal ends of cell–cell junctions (Figure 7M). These results are similar to observations in suspended cell pairs (Engl *et al.*, 2014). Not surprisingly, the average lifetime of EcadTSMod donor fluorophore (mTFP1) was evenly distributed along the junction (Figure 7N).

E-cadherin at distal ends of cell–cell junctions anchored to the actin cortex is believed to play a major role in the force propagation across the cell–cell junction (Maruthamuthu *et al.*, 2011) and may be recruited to the junction in a force-dependent manner. Thus we tested whether E-cadherin intensity along the entire junction or just the distal ends correlated with cell–cell forces. The distal ends of the cell–cell junction were defined by the ~3-μm width of actin bundles normal to the edges of cell–cell junctions. Cell–cell forces correlated poorly with E-cadherin intensity along the entire cell–cell junction and distal ends ($\rho = -0.14$ for the entire cell–cell junction [Supplemental Figure S3], and $\rho = 0.15$ for the distal ends [Supplemental Figure S8A]). A scatter plot of EcadTSMod FRET versus average E-cadherin–DsRed intensity at the distal ends on rectangles (Supplemental Figure S8B) revealed no significant correlation ($\rho = 0.08$). These data indicate that E-cadherin molecular tension is constant along the length of cell–cell junctions but that locally increased levels of E-cadherin support increased intercellular forces at the distal ends of cell–cell junction, as suggested by the CD-induced actin disassembly experiments (Figure 7).

DISCUSSION

Mechanotransduction at integrin-based focal adhesions has been well studied in single cells. In contrast, little is known about the mechanical interplay between cell–ECM and cell–cell adhesions in multicell conditions. In our reductionist model system, we examine pairs of MDCK epithelial cells adhering to rectangular and I-shaped ECM patterns designed to manipulate the force balance within cell pairs by varying the spatial distribution of cell–ECM adhesions and cell shape and size (Figures 1–4). We leveraged the findings of Tseng *et al.* (2012) that cell pairs preferentially align cell–cell junctions over areas with minimal ECM to engineer conditions in which cell–cell forces increased (isometric area dilation on rectangles) or remained constant (varying aspect ratio on I-shapes versus rectangles) with increasing cell–ECM forces.

Our findings of increased cell–cell and cell–ECM forces with isometric dilation of rectangular patterns is consistent with observations of unpatterned epithelial cell pairs having a range of spread areas (Maruthamuthu *et al.*, 2011). Increased total force with increasing area of patterned cell pairs was also consistent with prior observations that total traction forces increased in single patterned fibroblasts with increasing cell spread area and aspect ratio (Tan *et al.*, 2003; Oakes *et al.*, 2014). We further showed that changes in cell–cell and cell–ECM forces and overall strain energy in epithelial cell pairs were independent of the focal adhesion area, consistent with prior work using single patterned fibroblasts (Maruthamuthu *et al.*, 2011). Liu *et al.* (2010) observed that cell–cell force correlated with cell–cell junction length in endothelial cell pairs, but this trend was not observed in studies using unpatterned epithelial cell pairs (Maruthamuthu *et al.*, 2011). In our study of patterned epithelial cell pairs, we found that the cell–cell junction length decreased on I-shapes with sustained cell–cell forces and remained constant on rectangles with increasing cell–cell forces, presumably because rectangle patterns allowed cell–ECM adhesion at the distal edges of the cell–cell junctions (Figures 2 and 4). However, epithelial and endothelial cells also exhibit differences in their actin cytoskeleton that may contribute to the observed differences between these studies; for example, endothelial cells generate actin stress fibers, whereas epithelial cells form cortical bundles of actin (Stapleton *et al.*, 2014). Differences in the stiffness and porosity of PDMS micropost arrays (Liu *et al.*, 2010) versus continuous PAA hydrogels (Maruthamuthu *et al.*, 2011) may also affect the results (Schoen *et al.*, 2013).

Of importance, we found that cell–cell force was uncoupled from cell–ECM force when cell–ECM adhesions were absent from the distal edges of the cell–cell junctions. On I-shapes, cell–ECM focal adhesions formed exclusively on the distal bars and did not constrain cell–cell junction length (Figure 3), whereas they formed around the entire periphery of cell pairs on rectangles (Supplemental Figure S1B). Previous studies on the dynamics of epithelial cell–cell contact formation showed that localized Rho and Rac activity controls actomyosin-driven expansion of the E-cadherin junctions and that integrin-based adhesions are excluded beneath the center of E-cadherin junctions and localized to the edges of cell–cell contacts (Yamada and Nelson, 2007). Cell pairs on rectangles reproduced this organization of cell–cell and cell–ECM adhesions at cell–cell junctions and stabilized the junction length, whereas both cell–cell and cell–ECM forces increased as spread area increased.

To test whether cell–cell force was correlated with molecular tension on E-cadherin, we used a genetically encoded tension sensor, EcadTSMod. Previous EcadTSMod FRET measurements revealed that membrane-bound E-cadherin is under constitutive actomyosin-mediated tension and that molecular tension on E-cadherin at a cell–cell contact is transiently elevated by applying acute external elongations >200% of the initial length of cell pairs (Grashoff *et al.*, 2010; Borghi *et al.*, 2012). In this study, we used EcadTSMod to determine whether cell–cell junctions in cell pairs that were chronically "elongated" on adhesive rectangles or I-shapes experienced changes in the resting tension of E-cadherin while modulating the endogenous force balance of cell–cell and cell–ECM forces. Surprisingly, EcadTSMod FRET efficiency remained constant at 20% on 1:1.7 rectangles, and junction length remained constant and cell–cell force increased 2.5-fold compared with that on a 1:1 square (Figure 6). EcadTSMod FRET efficiency did not change in cell pairs over a range of elongated I-shapes, whereas junction length decreased and cell–cell force remained constant (Figure 6). The FRET efficiency of 20% was within the dynamic range of the TSMod tension sensor to detect molecular forces of 1–5 pN (Figure 6; Grashoff *et al.*, 2010).

Molecular-scale tension on E-cadherin was distributed evenly along the cell–cell junction; however, E-cadherin intensity levels were highest at the distal ends of cell–cell contacts (Figure 7M; Yamada and Nelson, 2007; Engl *et al.*, 2014). These results indicate that MDCK cells can maintain molecular tension homeostasis on E-cadherin over a range of cellular forces. Elevated forces acting across the cell–cell contact did not lead to an increase of force per molecule but shifted the spatial distribution of E-cadherin along the cell–cell junction to higher levels at the distal ends. This result agrees with recent work showing that E-cadherin does not affect the magnitude of cell–cell forces but the rate that cells within epithelial microtissues build up cell–cell forces (Bazellières *et al.*, 2015). Comparing traction forces between cell pairs and single cells constrained to the same pattern size, we found that the cell pairs exerted 2.5-fold-larger tractions than single cells (Figure 5). Surprisingly, the traction forces for each cell within cell pairs were also 2.2-fold higher than for single cells of comparable size, indicating that the presence of a cell–cell contact critically enhances cell traction forces.

We hypothesize that E-cadherin tension homeostasis could be facilitated through 1) recruitment of more E-cadherin to distribute the cell–cell force across more molecules, 2) recruitment of other classes of cell adhesion proteins such as desmosomes, or 3) variable interactions and spatial engagement of adhesion proteins with the cytoskeleton. We reject the first hypothesis because the average intensity of fluorescently tagged E-cadherin correlated weakly (and negatively in most cases) with increased cell–cell force or force per junction length when we varied the aspect ratio of the rectangle patterns and I-shapes (Figures 2D, 3E, and 4D and Supplemental Figures S3 and S8). We also reject the second hypothesis, since we observed a negative correlation between the staining intensity of desmoplakin, a component of desmosomes, and cell–cell force (Supplemental Figure S5). However, it is important to note that although these data do not support protein recruitment mechanisms, they do not rule them out conclusively. Fluorescence intensity measurements are not a quantitative proxy for protein density, and we only evaluated the fluorescence intensities of E-cadherin and desmoplakin. Lacking knowledge of the E-cadherin density, we also cannot use the molecular FRET signal of cytoplasmic EcadTSMod to estimate junctional forces. A more detailed analysis of additional adhesion proteins, their cytoplasmic adaptor proteins, and binding dynamics is needed to test the first two hypotheses completely, but this is beyond the scope of the present analysis.

Although E-cadherin molecular FRET homeostasis under large variations in cell–cell forces was unexpected, it also remains unexplained. Thus we considered the third hypothesis and examined the dynamic organization of E-cadherin and the actin cytoskeleton at the cell–cell junction using low concentrations of CD and ML-7 (Supplemental Figure S7). Similar retraction rates of actin filaments and E-cadherin plaques localized at the ends of the cell–cell junctions on both rectangles and I-shapes indicated force localization and tight association of actin filament bundles and E-cadherin (Figure 7). This tight association of E-cadherin and actin filaments is consistent with work showing that actin dynamics and myosin II contractility modulate E-cadherin immobilization to cell–cell contacts in suspended epithelial cell pairs (Engl *et al.*, 2014).

During maturation of E-cadherin cell–cell contacts, remodeling of the actin cytoskeleton controls the reorganization of mobile E-cadherin puncta into compacted, less mobile cell–cell contacts and E-cadherin plaques at the margins of the cell–cell junction (Adams *et al.*, 1998). Although we conclude that variable interactions and spatial engagement of adhesion proteins with the cytoskeleton do play a role in the endogenous cell–cell and cell–ECM force balance and E-cadherin molecular tension homeostasis, the mechanisms of reinforcement, whether by recruitment or activation of accessory proteins by conformational changes under load, remain unclear. It will be important in future investigations to leverage quantitative engineering and biological tools to explore the underlying mechanisms and mechanobiological set points.

MATERIALS AND METHODS

Cell culture and epifluorescence microscopy

MDCK type II G cells stably expressing fluorescently tagged proteins were maintained in low-glucose DMEM (11885; Invitrogen, Carlsbad, CA) containing 1 g/l sodium bicarbonate and supplemented with 10% (vol/vol) fetal bovine serum (FBS) and antibiotics as described previously (Borghi *et al.*, 2012). MDCK cells were transfected with the EcadTSMod FRET construct using Lipofectamine 2000 (11668027; Invitrogen) according to the manufacturer's instructions. Transfected cells were selected in 0.5g/l G418. Cells were washed and trypsinized in phosphate-buffered saline (PBS; pH 7.4), seeded, and incubated on the patterned gels for 16 h before live-cell imaging or fixation in 4% paraformaldehyde. For pharmacological perturbation, 0.5 μM cytochalasin D or 25 μM ML-7 was added (Yamada and Nelson, 2007). Cells were imaged on a Leica DMI 6000B inverted microscope with a xenon arc lamp (DG4 300W; Sutter Instruments, Novato, CA) and a 63×/numerical aperture 1.4 oil immersion objective (Leica). To reduce background fluorescence, phenol red–free Leibovitz's L-15 medium supplemented with 10% (vol/vol) FBS was used.

Micropatterning of polyacrylamide gels

A mixture of collagen I and fluorescently labeled gelatin was patterned on glass coverslips using a photoresist-assisted-liftoff technique (Möller *et al.*, 2013). Standard contact photolithography of S1818 photoresist (Microchem, Newton, MA) was used to fabricate photoresist-patterned glass coverslips. Coverslips were incubated with 0.1 mg/ml poly(L-lysine)-graft-poly(ethylene glycol) (PLL-g[3.5]-PEG(2 kDa); Surface Solutions, Zurich, Switzerland) for 1 h before 1-methylpyrrolidone–assisted photoresist lift-off. PLL-g-PEG patterns were backfilled with a mixture of 10 μg/ml Alexa Fluor 488–labeled gelatin (A-20173, Invitrogen; G1393, Sigma-Aldrich, St. Louis, MO) and 50 μg/ml collagen I (A1048301; Life Technologies, Gaithersburg, MD). Labeled gelatin was used instead of collagen because the low pH of the collagen solution was incompatible with the labeling protocol. To transfer the protein pattern, a 25-kPa PAA gel (0.5 g/ml acrylamide, 0.025 g/ml Bis-acrylamide) was polymerized between a protein-patterned glass coverslip and glass-bottom dish (MatTek, Ashland, MA) silanized with 3-(trimethoxysilyl)propyl methacrylate (M6514, Sigma-Aldrich; Supplemental Figure S1).

Fluorescence lifetime imaging microscopy

FLIM measurements of the FRET donor mTFP1 were performed with a Leica SP5 multiphoton microscope and Simple-Tau 152 single-photon counting system (Becker & Hickl, Berlin, Germany) consisting of Spectra Physics MaiTai, DeepSee ultrafast two-photon pulsed laser, and an external HPM-100-40 high-speed hybrid PMT/GaAsP detector. An HCX APO L20×/1.00 water immersion objective with 870-nm multiphoton excitation at 400 MHz and 512 × 512 pixel window was used for data acquisition. Photons were accumulated for up to 150 frames (3 min; Becker *et al.*, 2014). Time-domain FLIM experiments and FLIM data analysis were performed as described previously (Grashoff *et al.*, 2010) using SPCImage software (Becker & Hickl) and Matlab (MathWorks, Natick, MA). Fluorescence lifetimes were determined by fitting a double-exponential decay model. FRET efficiency was calculated from the equation FRET

efficiency = $1 - \tau/\tau_{donor}$, where τ is the lifetime of mTFP1 in the E-cadherin FRET sensor as a weighted-average lifetime from SPCImage software and τ_{donor} is the lifetime of mTFP1 alone, as described previously (Grashoff *et al.*, 2010).

Traction force microscopy

Fluorescent beads of size 0.2 µm were mixed in the 25-kPa PAA gels at 3% (vol/vol) from a stock solution (0.2 µm blue fluorescent, F-8805; Invitrogen). Images of fluorescent beads were taken with and without adherent cells and registered to correct stage drift using the ImageJ plug-in Template Matching and Slice Alignment (Tseng *et al.*, 2012). Cells were removed with 0.05% (wt/vol) trypsin for 10 min, followed by PBS wash. Bead displacements were detected using the Particle image velocimetry ImageJ plug-in (Tseng *et al.*, 2012) based on the cross-correlation algorithm with the final window size of 1.63 µm × 1.63 µm.

For each cell in the cell pair, cell–cell force was calculated as the vector sum of all tractions, and cell–ECM force was calculated by integrating the magnitude of forces parallel to the cell–cell junction using the Fourier transform traction cytometry ImageJ plug-in (Tseng *et al.*, 2012) with a regularization parameter of 1×10^{-9}. The strain energy was calculated over the entire cell pair as $U = \frac{1}{2}\int \vec{T} \cdot \vec{u}\, dA = \frac{1}{2}\sum \vec{F} \cdot \vec{u}$, where $\vec{T}$ is the traction stress and $\vec{u}$ is the bead displacement.

ACKNOWLEDGMENTS

We thank lab members and our joint mechanobiology group for insightful discussions. This material is based on work supported in part by Stanford Bio-X, the National Science Foundation (EFRI-1136790), the National Institutes of Health (EB-006745, GM-35527, 1DP2OD007078-01, T32 GM007276), European Research Council Advanced Grant 231157, the Burroughs-Wellcome CASI, and graduate research fellowships from the National Science Foundation, Stanford BioX, and the Ilju Foundation.

REFERENCES

Adams CL, Chen Y-T, Smith SJ, James Nelson W (1998). Mechanisms of epithelial cell–cell adhesion and cell compaction revealed by high-resolution tracking of E-cadherin-green fluorescent protein. J Cell Biol 142, 1105–1119.

Barry AK, Tabdili H, Muhamed I, Wu J, Shashikanth N, Gomez GA, Yap AS, Gottardi CJ, de Rooij J, Wang N, *et al.* (2014). α-Catenin cytomechanics—role in cadherin-dependent adhesion and mechanotransduction. J Cell Sci 127, 1779–1791.

Bazellières E, Conte V, Elosegui-Artola A, Serra-Picamal X, Bintanel-Morcillo M, Roca-Cusachs P, Muñoz JJ, Sales-Pardo M, Guimerà R, Trepat X (2015). Control of cell–cell forces and collective cell dynamics by the intercellular adhesome. Nat Cell Biol 17, 409–420.

Becker W, Shcheslavkiy V, Frere S, Slutsky I (2014). Spatially resolved recording of transient fluorescence-lifetime effects by line-scanning TCSPC. Microsc Res Tech 77, 216–224.

Borghi N, Sorokina M, Shcherbakova OG, Weis WI, Pruitt BL, Nelson WJ, Dunn AR (2012). E-cadherin is under constitutive actomyosin-generated tension that is increased at cell–cell contacts upon externally applied stretch. Proc Natl Acad Sci USA 109, 12568–12573.

Buckley CD, Tan J, Anderson KL, Hanein D, Volkmann N, Weis WI, Nelson WJ, Dunn AR (2014). The minimal cadherin-catenin complex binds to actin filaments under force. Science 346, 1254211.

Butler JP, Tolić-Nørrelykke IM, Fabry B, Fredberg JJ (2002). Traction fields, moments, and strain energy that cells exert on their surroundings. Am J Physiol Cell Physiol 282, C595–C605.

Cai D, Chen S-C, Prasad M, He L, Wang X, Choesmel-Cadamuro V, Sawyer JK, Danuser G, Montell DJ (2014). Mechanical feedback through E-cadherin promotes direction sensing during collective cell migration. Cell 157, 1146–1159.

Chu Y-S, Thomas WA, Eder O, Pincet F, Perez E, Thiery JP, Dufour S (2004). Force measurements in E-cadherin-mediated cell doublets reveal rapid adhesion strengthened by actin cytoskeleton remodeling through Rac and Cdc42. J Cell Biol 167, 1183–1194.

Drees F, Pokutta S, Yamada S, Nelson WJ, Weis WI (2005). α-Catenin is a molecular switch that binds E-cadherin-β-catenin and regulates actin-filament assembly. Cell 123, 903–915.

Engl W, Arasi B, Yap LL, Thiery JP, Viasnoff V (2014). Actin dynamics modulate mechanosensitive immobilization of E-cadherin at adherens junctions. Nat Cell Biol 16, 587–594.

Friedl P, Gilmour D (2009). Collective cell migration in morphogenesis, regeneration and cancer. Nat Rev Mol Cell Biol 10, 445–457.

Ghibaudo M, Saez A, Trichet L, Xayaphoummine A, Browaeys J, Silberzan P, Buguin A, Ladoux B (2008). Traction forces and rigidity sensing regulate cell functions. Soft Matter 4, 1836–1843.

Grashoff C, Hoffman BD, Brenner MD, Zhou R, Parsons M, Yang MT, McLean MA, Sligar SG, Chen CS, Ha T, *et al.* (2010). Measuring mechanical tension across vinculin reveals regulation of focal adhesion dynamics. Nature 466, 263–266.

Halbleib JM, Nelson WJ (2006). Cadherins in development: cell adhesion, sorting, and tissue morphogenesis. Genes Dev 20, 3199–3214.

le Duc Q, Shi Q, Blonk I, Sonnenberg A, Wang N, Leckband D, Rooij J de (2010). Vinculin potentiates E-cadherin mechanosensing and is recruited to actin-anchored sites within adherens junctions in a myosin II–dependent manner. J Cell Biol 189, 1107–1115.

Liu Z, Tan JL, Cohen DM, Yang MT, Sniadecki NJ, Ruiz SA, Nelson CM, Chen CS (2010). Mechanical tugging force regulates the size of cell–cell junctions. Proc Natl Acad Sci USA 107, 9944–9949.

Maruthamuthu V, Sabass B, Schwarz US, Gardel ML (2011). Cell-ECM traction force modulates endogenous tension at cell–cell contacts. Proc Natl Acad Sci USA 108, 4708–4713.

Möller J, Emge P, Vizcarra IA, Kollmannsberger P, Vogel V (2013). Bacterial filamentation accelerates colonization of adhesive spots embedded in biopassive surfaces. New J Phys 15, 125016.

Oakes PW, Banerjee S, Marchetti MC, Gardel ML (2014). Geometry regulates traction stresses in adherent cells. Biophys J 107, 825–833.

Rape AD, Guo W, Wang Y (2011). The regulation of traction force in relation to cell shape and focal adhesions. Biomaterials 32, 2043–2051.

Rossier OM, Gauthier N, Biais N, Vonnegut W, Fardin MA, Avigan P, Heller ER, Mathur A, Ghassemi S, Koeckert MS, *et al.* (2010). Force generated by actomyosin contraction builds bridges between adhesive contacts. EMBO J 29, 1055–1068.

Schoen I, Pruitt BL, Vogel V (2013). The yin-yang of rigidity sensing: how forces and mechanical properties regulate the cellular response to materials. Annu Rev Mater Res 43, 589–618.

Stapleton SC, Chopra A, Chen CS (2014). Force measurement tools to explore cadherin mechanotransduction. Cell Commun Adhes 21, 193–205.

Takeichi M (2014). Dynamic contacts: rearranging adherens junctions to drive epithelial remodelling. Nat Rev Mol Cell Biol 15, 397–410.

Tambe DT, Croutelle U, Trepat X, Park CY, Kim JH, Millet E, Butler JP, Fredberg JJ (2013). Monolayer stress microscopy: limitations, artifacts, and accuracy of recovered intercellular stresses. PLoS One 8, e55172.

Tambe DT, Hardin CC, Angelini TE, Rajendran K, Park CY, Serra-Picamal X, Zhou EH, Zaman MH, Butler JP, Weitz DA, *et al.* (2011). Collective cell guidance by cooperative intercellular forces. Nat Mater 10, 469–475.

Tan JL, Tien J, Pirone DM, Gray DS, Bhadriraju K, Chen CS (2003). Cells lying on a bed of microneedles: an approach to isolate mechanical force. Proc Natl Acad Sci USA 100, 1484–1489.

Tee S-Y, Fu J, Chen CS, Janmey PA (2011). Cell shape and substrate rigidity both regulate cell stiffness. Biophys J 100, L25–L27.

Tseng Q, Duchemin-Pelletier E, Deshiere A, Balland M, Guillou H, Filhol O, Théry M (2012). Spatial organization of the extracellular matrix regulates cell–cell junction positioning. Proc Natl Acad Sci USA 109, 1506–1511.

Twiss F, Duc QL, Horst SVD, Tabdili H, Krogt GVD, Wang N, Rehmann H, Huveneers S, Leckband DE, Rooij JD (2012). Vinculin-dependent Cadherin mechanosensing regulates efficient epithelial barrier formation. Biol Open 1, 1128–1140.

Vogel V, Sheetz M (2006). Local force and geometry sensing regulate cell functions. Nat Rev Mol Cell Biol 7, 265–275.

Yamada S, Nelson WJ (2007). Localized zones of Rho and Rac activities drive initiation and expansion of epithelial cell–cell adhesion. J Cell Biol 178, 517–527.

Yonemura S, Wada Y, Watanabe T, Nagafuchi A, Shibata M (2010). α-Catenin as a tension transducer that induces adherens junction development. Nat Cell Biol 12, 533–542.

Zimmermann J, Hayes RL, Basan M, Onuchic JN, Rappel W-J, Levine H (2014). Intercellular stress reconstitution from traction force data. Biophys J 107, 548–554.